



TITLE:

Single-neutron knockout from [20]C and the structure of [19]C

AUTHOR(S):

Hwang, J.W.; Kim, S.; Satou, Y.; Orr, N.A.; Kondo, Y.; Nakamura, T.; Gibelin, J.; ... Tuff, A.G.; Vandebrouck, M.; Yoneda, K.

CITATION:

Hwang, J.W. ...[et al]. Single-neutron knockout from [20]C and the structure of [19]C. Physics Letters B 2017, 769(10): 503-508

ISSUE DATE:

2017-06-10

URL:

<http://hdl.handle.net/2433/227706>

RIGHT:

©2017 The Author(s). Published by Elsevier B.V. This is an open access article under the CC BY license (<http://creativecommons.org/licenses/by/4.0/>). Funded by SCOAP3.



Contents lists available at ScienceDirect

Physics Letters B

www.elsevier.com/locate/physletb



Single-neutron knockout from ^{20}C and the structure of ^{19}C



J.W. Hwang^{a,*}, S. Kim^a, Y. Satou^a, N.A. Orr^b, Y. Kondo^c, T. Nakamura^c, J. Gibelin^b, N.L. Achouri^b, T. Aumann^{d,e}, H. Baba^f, F. Delaunay^b, P. Doornenbal^f, N. Fukuda^f, N. Inabe^f, T. Isobe^f, D. Kameda^f, D. Kanno^c, N. Kobayashi^c, T. Kobayashi^g, T. Kubo^f, S. Leblond^b, J. Lee^{f,1}, F.M. Marqués^b, R. Minakata^c, T. Motobayashi^f, D. Murai^h, T. Murakamiⁱ, K. Muto^g, T. Nakashima^c, N. Nakatsukaⁱ, A. Navin^j, S. Nishi^c, S. Ogoshi^c, H. Otsu^f, H. Sato^f, Y. Shimizu^f, H. Suzuki^f, K. Takahashi^g, H. Takeda^f, S. Takeuchi^f, R. Tanaka^c, Y. Togano^e, A.G. Tuff^k, M. Vandebrouck^l, K. Yoneda^f

^a Department of Physics and Astronomy, Seoul National University, 1 Gwanak-ro, Gwanak-gu, Seoul 08826, Republic of Korea

^b LPC-Caen, IN2P3/CNRS, ENSICAEN, UNICAEN et Normandie Université, 14050 Caen Cedex, France

^c Department of Physics, Tokyo Institute of Technology, 2-12-1 O-Okayama, Meguro, Tokyo 152-8551, Japan

^d Institut für Kernphysik, Technische Universität Darmstadt, D-64289 Darmstadt, Germany

^e ExtreMe Matter Institute EMMI and Research Division, GSI Helmholtzzentrum für Schwerionenforschung GmbH, D-64291 Darmstadt, Germany

^f RIKEN Nishina Center, Hirosawa 2-1, Wako, Saitama 351-0198, Japan

^g Department of Physics, Tohoku University, Miyagi 980-8578, Japan

^h Department of Physics, Rikkyo University, Toshima, Tokyo 171-8501, Japan

ⁱ Department of Physics, Kyoto University, Kyoto 606-8502, Japan

^j GANIL, CEA/DRF-CNRS/IN2P3, F-14076 Caen Cedex 5, France

^k Department of Physics, University of York, Heslington, York YO10 5DD, United Kingdom

^l Institut de Physique Nucléaire, Université Paris-Sud, IN2P3/CNRS, 91406 Orsay, France

ARTICLE INFO

Article history:

Received 16 December 2016

Received in revised form 16 March 2017

Accepted 10 April 2017

Available online 13 April 2017

Editor: D.F. Geesaman

Keywords:

Heavy-ion knockout

Invariant mass spectroscopy

Shell evolution

ABSTRACT

The low-lying unbound level structure of the halo nucleus ^{19}C has been investigated using single-neutron knockout from ^{20}C on a carbon target at 280 MeV/nucleon. The invariant mass spectrum, derived from the momenta of the forward going beam velocity ^{18}C fragment and neutrons, was found to be dominated by a very narrow near threshold ($E_{\text{rel}} = 0.036(1)$ MeV) peak. Two less strongly populated resonance-like features were also observed at $E_{\text{rel}} = 0.84(4)$ and $2.31(3)$ MeV, both of which exhibit characteristics consistent with neutron p -shell hole states. Comparisons of the energies, measured cross sections and parallel momentum distributions to the results of shell-model and eikonal reaction calculations lead to spin-parity assignments of $5/2_1^+$ and $1/2_1^-$ for the levels at $E_x = 0.62(9)$ and $2.89(10)$ MeV with $S_n = 0.58(9)$ MeV. Spectroscopic factors were also deduced and found to be in reasonable accord with shell-model calculations. The valence neutron configuration of the ^{20}C ground state is thus seen to include, in addition to the known $1s_{1/2}^2$ component, a significant $0d_{5/2}^2$ contribution. The level scheme of ^{19}C , including significantly the $1/2_1^-$ cross-shell state, is well accounted for by the YSOX shell-model interaction developed from the monopole-based universal interaction.

© 2017 The Author(s). Published by Elsevier B.V. This is an open access article under the CC BY license (<http://creativecommons.org/licenses/by/4.0/>). Funded by SCOAP³.

The atomic nucleus is a finite fermionic quantum system that exhibits shell structure. The manner and mechanisms by which this evolves with the neutron–proton (N/Z) asymmetry across the nuclear landscape is one of the key questions in nuclear structure physics. Such investigations may be traced back to the early work

of Talmi and Unna [1] where the ordering of the lowest-lying levels in ^{11}Be and ^{15}C was discussed in terms of the residual shell-model interaction [2]. Since these pioneering studies, the p - sd -shell nuclei have provided an important testing ground to explore our understanding of shell structure away from stability. Experimentally, such studies are now possible beyond the proton and neutron driplines, as evidenced by recent measurements of the most exotic oxygen isotopes [3–7]. Theoretically, the description of such near-drip-line nuclei is now possible using sophisticated models,

* Corresponding author.

E-mail address: hjw8707@snu.ac.kr (J.W. Hwang).

¹ Present address: Department of Physics, University of Hong Kong, Pokfulam Road, Hong Kong.

ranging from the shell model to *ab initio* approaches, which include, explicitly or implicitly effects, such as three-nucleon forces, the continuum (and coupling to it for weakly bound levels), and tensor forces (see, for example, Refs. [8–12]).

Of particular note in the context of the work presented here are shell-model calculations employing effective interactions derived from *ab initio* coupled-cluster (CCEI) theory which are now capable of predicting the binding energies and low-lying levels for the most neutron-rich carbon and oxygen isotopes [10]. In contrast, Otsuka et al. have constructed a monopole-based universal interaction (V_{MU}) consisting of the central and $\pi + \rho$ tensor terms [11] which has provided intriguing insight into changes in shell structure, including the neutron-rich *p*-*sd*-shell nuclei [12]. This Letter reports the observation of $5/2^+$ and $1/2^-$ states in ^{19}C populated via single-neutron knockout from ^{20}C at 280 MeV/nucleon. The results are discussed in the context of a range of shell-model calculations, including those just mentioned, and conclusions are drawn regarding the underlying shell structure. Importantly, the observation of the $1/2^-$ neutron *p*-shell hole state provides a direct test of the cross-shell components of the shell-model interactions.

The nucleus ^{19}C is the heaviest bound odd-*A* carbon isotope and the lightest member of the $N = 13$ isotonic chain. Structurally it is one of the few well established single-neutron halo nuclei [13–15] with a very weakly bound *s*-wave valence neutron ($S_n = 0.58(9)$ MeV [16]) and ground state spin-parity $J^\pi = 1/2^+$ [17,18]. The low-lying level structure of ^{19}C is expected to be composed of $1/2^+$, $3/2^+$, and $5/2^+$ states, arising from neutron occupancy of the almost degenerate $0d_{5/2}$ and $1s_{1/2}$ orbitals [19]. Although most shell-model predictions suggest that these states are closely spaced and located well below 1 MeV, their ordering has been the subject of considerable uncertainty including, in particular, the location of the $5/2_1^+$ level.

The first in-beam γ -ray spectroscopy of ^{19}C employed the (*p*, *p'*) reaction in inverse kinematics, and identified cascade transitions consistent with two bound excited states at 0.196(6) and 0.269(8) MeV [20], which were tentatively assigned $3/2^+$ and $5/2^+$, respectively. A measurement employing fragmentation of a mixed secondary beam confirmed the existence of the transition from the $3/2^+$ state to the ground state [19]. A subsequent invariant mass study, also using the (*p*, *p'*) reaction in inverse kinematics, observed an unbound level at 1.46(10) MeV, the angular distribution of which was consistent with a $5/2^+$ state [21]. More recently, investigations of inclusive two-neutron removal from ^{20}C suggested, through comparison with eikonal reaction model calculations and shell-model spectroscopic factors, that the $5/2_1^+$ state should be unbound [22,23], in contradiction with the conclusions of Ref. [20]. Subsequently a candidate for the $5/2_1^+$ state was observed just above threshold ($E_x = 0.693(95)$ MeV) in the $^{18}\text{C} + \text{neutron}$ invariant mass spectrum following multi-nucleon removal from ^{22}N [24].²

Recently two further in-beam γ -ray measurements were reported [25,26]. Both confirmed the existence of a level, assigned $3/2^+$, at 0.20 MeV, whilst the former also provided a measure of the lifetime and $B(M1)$ strength. In summary, the lowest two states – the ground $1/2_1^+$ halo state and the $3/2_1^+$ level at 0.20 MeV – are bound, whilst the $5/2_1^+$ state most probably lies just above the neutron decay threshold. As will be discussed, the present work confirms this conjecture (and provides a clear *d*-wave assignment) and observes two more higher-lying resonances, one of which is identified as the lowest-lying negative parity state in ^{19}C .

² The tentative $5/2_1^+$ assignment was based on a comparison with shell-model excitation energies.

In terms of the ^{20}C projectile, the momentum distribution and the associated cross section for the $\text{C}(^{20}\text{C}, ^{19}\text{C})$ reaction, in the aforementioned inclusive neutron removal study [23], reveal the presence of a significant $1s_{1/2}^2$ valence neutron configuration. The expected $0d_{5/2}^2$ component was not probed, as the corresponding $5/2^+$ level in ^{19}C is, as noted above, unbound. It is worthwhile noting that the structure of ^{20}C is of interest, not only in terms of shell evolution around the $N = 14$ sub-shell closure [19], but as the core of the heaviest two-neutron halo system ^{22}C [27,28].

The experiment was performed at the Radioactive Isotope Beam Factory (RIBF) [29] of the RIKEN Nishina Center as a part of a series of measurements investigating the structure of light neutron-rich nuclei beyond the dripline (see, for example, Ref. [7]). A 345 MeV/nucleon ^{48}Ca primary beam (~ 100 pA) impinging on a 20 mm-thick Be production target was employed, in conjunction with the BigRIPS separator [30], to produce a mixed secondary beam, including ^{20}C at an average rate of 190 pps. The various isotopes present in the secondary beam were identified event-by-event using measurements of the energy loss, time-of-flight, and magnetic rigidity. The secondary beam was transported to the object point of the SAMURAI spectrometer [31] where a carbon reaction target with a thickness of 1.8 g/cm² was located. The beam particles were tracked onto the target using two drift chambers. The ^{20}C mid-target energy was 280 MeV/nucleon. Data were also acquired with the carbon target removed in order to account for reactions in the various beam detectors.

The forward-focused beam velocity reaction products, including ^{18}C and a neutron, were detected using the SAMURAI spectrometer and large area NEBULA neutron array [32]. The charged fragments were momentum analyzed by the 3 T superconducting dipole magnet, and the magnetic rigidity deduced using the trajectories derived from drift chambers placed at the entrance and exit of the magnet as described in Ref. [31]. A 16-element plastic hodoscope provided for energy loss and time-of-flight measurements, which combined with the rigidity permitted the charged fragments to be identified.

The NEBULA array was located some 11 m downstream of the secondary target. The array comprised 120 individual detector modules (each 12 cm \times 12 cm \times 180 cm) and 24 charged particle veto detectors (thickness 1 cm), arranged in a two-wall configuration, with an inter-wall separation of 85 cm. The neutron momenta were derived from the time-of-flight (measured with respect to a plastic detector placed forward of the secondary target) and hit position.

The γ rays emitted from excited states of the charged fragments were detected using 140 NaI(Tl) scintillators of the DALI2 array [33] which were arranged in a 4π -like configuration around the secondary reaction target. As such, the array had a detection efficiency of 16% at 1 MeV and an energy resolution (FWHM) of 150 keV.

The relative energy (E_{rel}) of $^{19}\text{C}^*$ was reconstructed from the four-momenta of the ^{18}C fragment and decay neutron. Specifically, the E_{rel} was calculated as,

$$E_{\text{rel}} = \sqrt{(E_f + E_n)^2 - |\mathbf{p}_f + \mathbf{p}_n|^2} - (M_f + M_n), \quad (1)$$

where E_f (E_n), \mathbf{p}_f (\mathbf{p}_n), and M_f (M_n) are the total energy, momentum, and mass of ^{18}C (neutron), respectively.

In the eikonal-model description of nucleon knockout, neutrons are removed from the ^{20}C projectile via absorption and diffraction [34]. At the present beam energies the former process dominates. The small fraction ($\sim 10\%$) of diffractive breakup events is associated with two beam-velocity neutrons in the outgoing channel in coincidence with ^{18}C . As such, a very broad low-level background

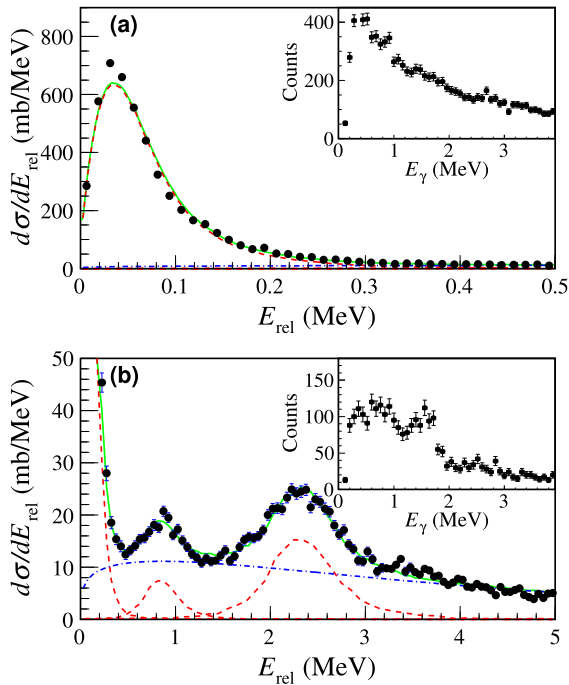


Fig. 1. (Color online.) Relative energy spectrum for the $^{18}\text{C} + n$ system (solid points with error bars) up to (a) 0.5 MeV and (b) 5 MeV. The solid (green) curve shows the results of the fit to the overall spectrum. The dashed (red) and dot-dashed (blue) curves represent the lineshapes of the individual resonances and background, respectively. The inset of panel (a) displays the Doppler-corrected energy spectrum of γ rays in coincidence with the threshold peak – $E_{\text{rel}} < 0.2$ MeV – while that of panel (b) the spectrum in coincidence with events in the range $E_{\text{rel}} = 0.5\text{--}1.3$ MeV.

[35], in addition to the $^{19}\text{C}^*$ continuum, is expected (as verified by simulations) in the E_{rel} spectrum.

The longitudinal momentum (p_{\parallel}) of $^{19}\text{C}^*$ was deduced from the sum of \mathbf{p}_f and \mathbf{p}_n after correcting for the spread in ^{20}C beam momenta. The p_{\parallel} and E_{rel} distributions shown in the following were obtained after subtracting the contributions arising from material other than the secondary reaction target.

The $^{18}\text{C} + n$ E_{rel} spectrum (Fig. 1) exhibits a very prominent narrow threshold peak together with two more weakly populated higher-lying structures. In order to display the results in terms of the differential cross section, $d\sigma/dE_{\text{rel}}$, the geometrical acceptances and detection efficiencies have been taken into account. The former were evaluated, as a function of E_{rel} , using a complete simulation of the setup, which included the characteristics of the ^{20}C secondary beam and the momentum imparted to $^{19}\text{C}^*$ by the knocked-out neutron.

In order to describe qualitatively the E_{rel} spectrum, three single-level R-matrix lineshapes [36], convoluted with the experimental resolution function, and a very broad distribution (representing the continuum and diffracted neutron background – see above) were employed, following similar procedures to those detailed in Ref. [21]. The resolution function, generated by simulations incorporating the effects of all the relevant detectors,³ varied as $(\text{FWHM}) \Delta E_{\text{rel}} \approx 0.40\sqrt{E_{\text{rel}}}$ MeV. The underlying continuum background distribution was modeled, in line with earlier work (see, for example, Ref. [37]), with a Maxwellian-like distribution with a functional form of $a\sqrt{x}e^{-bx}$, where $x = E_{\text{rel}}$, and a and b were the fitting parameters. It may be noted that the form of the continuum is rather strongly constrained by the minima at

0.5 and 1.4 MeV, the spectrum at high E_{rel} , and that the intensity at 0 MeV must be zero.

Resonance energies of 0.036(1), 0.84(4), and 2.31(3) MeV were deduced, where single-level R-matrix lineshapes [21] with $\ell_n = 1$ and 2 dependencies, according to the spin-parity assignments made below, were employed. In the case of the lowest two peaks the widths were dominated by the experimental resolution and only upper limits could be determined (Table 1). As no obvious coincident γ rays were observed for the $^{18}\text{C} + n$ events⁴ forming the near threshold and highest-lying peaks (the inset of Fig. 1(a) illustrates this for the threshold state) corresponding excitation energies in ^{19}C of 0.62(9) and 2.89(10) MeV, where the uncertainty in $S_n(^{19}\text{C})$ has been included, were deduced.

In the case of the most weakly populated peak at $E_{\text{rel}} = 0.84$ MeV, the coincident γ -ray spectrum (inset of Fig. 1(b)) shows evidence for the feeding of the $^{18}\text{C}(2_1^+)$ state. Taking into account the detection efficiencies and assuming that all of the observed 1.6 MeV γ rays are associated with the $E_{\text{rel}} = 0.84$ MeV peak and not the underlying continuum, a branching ratio of order 100% is deduced. This suggests that a higher-lying level is being populated. We return to the origin of this peak below.

Theoretically single-neutron removal cross section σ_{-1n} leading to a given final state can be expressed in a factorized form as [40],

$$\sigma_{-1n} = \sum_{nlj} \left(\frac{A}{A-1} \right)^N C^2 S(J^\pi, nlj) \sigma_{\text{sp}}(nlj, S_n^{\text{eff}}), \quad (2)$$

where σ_{sp} is the single-particle cross section, nlj denote the quantum numbers of the knocked-out neutron, $[A/(A-1)]^N$ is the center-of-mass correction factor with A the mass number of the projectile and N the principal oscillator quantum number ($N = 2n + \ell$) [41], and S_n^{eff} the effective one-neutron separation energy given by the sum of S_n of the projectile ($S_n(^{20}\text{C}) = 2.93(26)$ MeV [16]) and E_x of the state in question.

Shell-model spectroscopic factors ($C^2 S$) were computed using the NuSHELLX@MSU [42] code and the WBP interaction [38]⁵ in the $0p\text{--}1s0d$ model space (Table 1). The σ_{sp} and associated momentum distributions were computed using the MOMDIS code [43]. The valence neutron wave function was calculated using a Woods–Saxon potential and the well-depth prescription of Ref. [44]. The range parameter of the nucleon–nucleon profile function [45] at the present energy (280 MeV/nucleon) was set to zero [40].

The nucleon density distribution of the ^{19}C core was estimated from a Hartree–Fock calculation using the SkX interaction [46]. The density distribution of the carbon target was chosen to be of a Gaussian form with a point-nucleon rms radius of 2.32 fm. An overall uncertainty, not included in the tabulated values, of $\pm 15\%$ was assigned to σ_{sp} , comprising $\pm 10\%$ associated with uncertainties in the size of the unbound core (corresponding changes of the core radius of $\pm 5\%$) and $\pm 10\%$ arising from uncertainties in the reaction theory [47,48].

Fig. 2 shows the $^{19}\text{C}^*$ p_{\parallel} distributions in the laboratory frame, after account was taken for the underlying continuum background, for the well defined levels at $E_x = 0.62$ and 2.89 MeV together with the peak at $E_{\text{rel}} = 0.84$ MeV. More specifically, for each momentum bin, the E_{rel} spectrum was fit assuming the three peaks and the continuum background distribution. The error bars shown are statistical and the choice of the exact form for the continuum distribution did not change perceptibly the form of the extracted

⁴ $E_x(2_1^+) = 1.6$ MeV in ^{18}C [19,39].

⁵ Only small variations were found between the results obtained using the WBP, WBT, and YSOX interactions.

³ The NEBULA hit position and timing resolutions being the dominant contributions.

Table 1

Cross sections (σ_{-1n}) and excitation energies (E_x) of the unbound states in ^{19}C produced via single-neutron knockout from ^{20}C compared with reaction and shell-model (WBP interaction [38]) calculations. See text for discussion of the character of the peak at $E_{\text{rel}} = 0.84$ MeV.

E_{rel} (MeV)	E_x (MeV)	Γ (MeV)	ℓ (\hbar)	$\sigma_{-1n}^{\text{exp}}$ (mb)	σ_{sp} (mb) ^{a,b}	$C^2 S^{\text{exp}a}$	$C^2 S^{\text{th}}$	E_x^{th} (MeV)	J^π
0.036(1)	0.62(9)	< 0.015	2	61(5)	22.9	2.40(20)	3.80	0.240	$5/2_1^+$
0.84(4)	3.0–5.5 ^c	< 0.02	1	4(1)					
2.31(3)	2.89(10)	0.20(7)	1	15(3)	18.6	0.77(15)	1.38	1.907	$1/2_1^-$

^a An uncertainty, not tabulated, associated with the reaction modeling of $\pm 15\%$ is estimated for σ_{sp} and hence $C^2 S^{\text{exp}}$ (see text).

^b S_n^{eff} derived from the experimental E_x were employed in the reaction calculations.

^c See text.

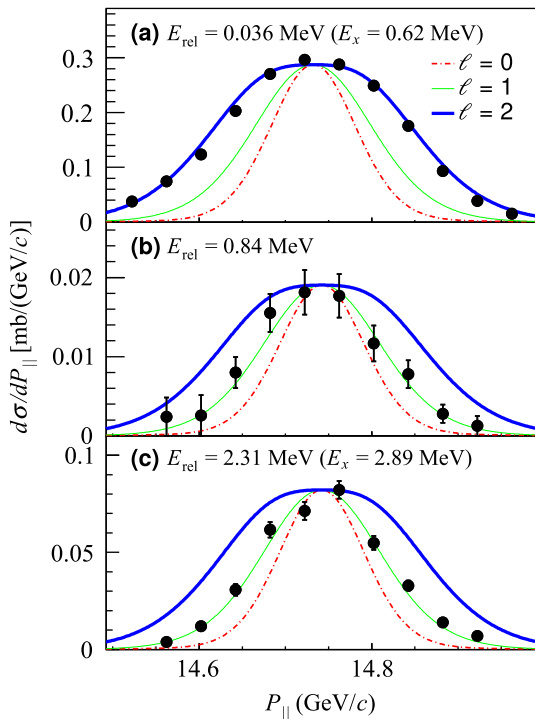


Fig. 2. (Color online.) Experimental longitudinal momentum distributions (solid points) compared with those computed for removal of neutrons with $\ell = 0, 1$, and 2 (red dot-dashed, green solid, and thick blue solid lines, respectively) for the states at $E_x = 0.62$ (a) and 2.89 MeV (c) and the peak at $E_{\text{rel}} = 0.84$ MeV (b). The theoretical lineshapes have been convoluted with the experimental resolution and, for the purpose of comparison, the lineshapes are normalized to that which best fits the measurements (see text).

momentum distributions. The experimental distributions are compared in each case in Fig. 2 with the theoretical lineshapes, convoluted with the experimental resolution ($\sigma \approx 28$ MeV/c in the beam rest frame), for removal of neutrons with orbital angular momentum $\ell = 0, 1$, and 2. In the case of the $E_x = 0.62$ MeV state, the data are very well described when the removed neutron is of d -wave character. The experimental distribution for the 2.89 MeV level is in very good agreement with removal of a p -wave neutron.

For the peak at $E_{\text{rel}} = 0.84$ MeV, the p_{\parallel} distribution is well reproduced assuming p -wave neutron removal ($\chi^2/n = 0.3, 3.0$ and 5.7 for $\ell = 1, 0$, and 2 respectively). Interestingly, the apparent excitation energy assuming no feeding of the $^{18}\text{C}(2_1^+)$ state is $1.42(10)$ MeV, very close to that of the $5/2_1^+$ level observed ($E_x = 1.46(10)$ MeV) in the (p, p') investigation [21], which, based on the WBP interaction spectroscopic factor and eikonal model, would be expected to be weakly populated (~ 3 mb). The incompatibility of the momentum distribution with d -wave neutron removal is consistent, however, with the suggestion derived from the γ -ray coincidences (see above) that this peak arises from pop-

ulation of a higher-lying level in ^{19}C which has a decay branch that proceeds via the $^{18}\text{C}(2_1^+)$ excited state, rather than through neutron emission directly to the ground state. It may also be noted that the neutron-decay width observed here ($\Gamma < 0.02$ MeV) is significantly smaller than in the inelastic scattering study [21].

Table 1 summarizes the results where the uncertainties quoted for E_x are dominated by the uncertainty in $S_n(^{19}\text{C})$. Those assigned to the cross sections ($\sigma_{-1n}^{\text{exp}}$) arise from the uncertainty in the exact form for the continuum background distribution (5%, 11%, and 17% for the $E_{\text{rel}} = 0.036, 0.84$, and 2.31 MeV resonances, respectively), the statistical uncertainty (2.5%, 8.3%, and 4.5%), the neutron detection efficiency (5% for all resonances), and geometrical acceptance (2%).

The energy of the state at $E_x = 0.62$ MeV is consistent with that reported by the multi-nucleon removal study of Ref. [24]. The clear $\ell = 2$ character of the momentum distribution and the large spectroscopic factor allow the state to be assigned as the $5/2_1^+$ with good confidence – the spectroscopic strength to $3/2^+$ levels is, unsurprisingly, expected to be very low ($C^2 S \lesssim 0.25$). The strong population of this level reflects the significant $0d_{5/2}^2$ valence neutron configuration in ^{20}C whereby the occupancy of the $0d_{5/2}$ neutron orbital is predicted to be around 4.3.⁶ It may also be noted that the unbound character of the $5/2_1^+$ level is in line with the earlier suggestions of Refs. [22–24,26].

The clear $\ell = 1$ character of the momentum distribution associated with the 2.89 MeV level indicates a spin-parity of $1/2^-$ or $3/2^-$. The moderate spectroscopic strength favors the $1/2^-$ assignment, which is reinforced by the location of the corresponding levels in $^{15,17}\text{C}$ [49–51]. As may be seen in Fig. 3, in both cases the $1/2_1^-$ state lies over 1 MeV below the $3/2_1^-$. In addition, the YSOX interaction (see below), which predicts very well the position of the $1/2_1^-$ level in $^{15,17}\text{C}$, indicates it should lie in ^{19}C very close to the energy observed here and, once again, well below the $3/2_1^-$.

In the case of the $E_{\text{rel}} = 0.84$ MeV peak, the $\ell = 1$ character of the associated momentum distribution and the energy difference of $1.47(5)$ MeV with respect to the relatively broad ($\Gamma = 0.20(7)$ MeV) $1/2^-$ level suggest that it could, in principle, arise from decay of the latter to the $^{18}\text{C}(2_1^+)$ state. Shell-model calculations indicate, however, that the branching ratio for such a decay is negligible and that the decay of the $1/2^-$ level proceeds essentially exclusively to the ^{18}C ground state.⁷

The shell-model predictions (Fig. 4) place the first $3/2^-$ state above ~ 3.0 MeV excitation energy. In terms of strength, the eikonal-model calculations suggest the cross section to be around half of that predicted for the population of the $1/2_1^-$ level. While

⁶ That of the $0d_{3/2}$ neutron orbital is predicted to be close to 0.5 and 1.3 for the $1s_{1/2}$ orbit.

⁷ Note that if such a scenario were the origin of the $E_{\text{rel}} = 0.84$ MeV peak, the increase in yield to the $E_x = 2.89$ MeV level would be similar to the experimental uncertainty (Table 1) and, in terms of the spectroscopic factor, much smaller than the uncertainty ascribed to the reaction modeling.

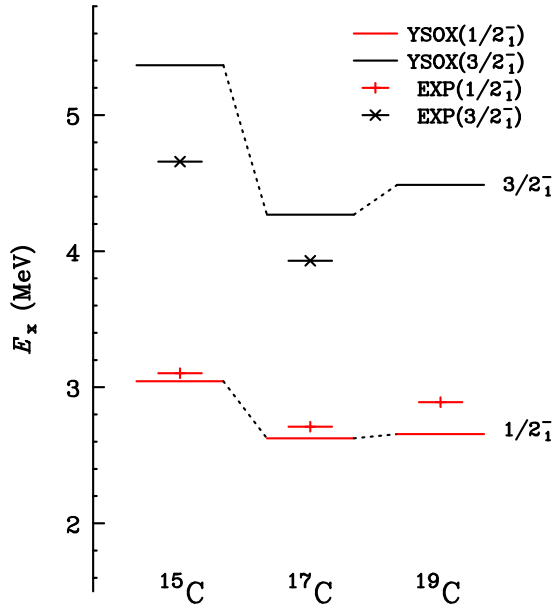


Fig. 3. (Color online.) Excitation energies of the $1/2^-$ (red) and $3/2^-$ (black) levels in $^{15,17}\text{C}$ [49–51] compared with shell-model calculations employing the YSOX interaction (see text). In the case of ^{19}C the $\ell = 1$ resonance observed here at 2.89 MeV is displayed together with the shell-model predictions.

the $3/2^-$ state is calculated to have a reasonably strong decay branch to the $^{18}\text{C}(2_1^+)$ level, placing it at $E_x = 3.02$ MeV, it is highly unlikely (see above and Fig. 3) that it is almost degenerate with the $1/2^-$ level.

Given then that the $3/2^-$ state almost certainly lies above the $1/2^-$, it is possible that the $E_{\text{rel}} = 0.84$ MeV peak could arise from decay to the $(0, 2)^+$ level(s) at 2.5 MeV in ^{18}C [19,52], with a corresponding excitation energy in ^{19}C of 3.92 MeV. While the shell-model calculations suggest that a reasonably strong decay branch to the $^{18}\text{C}(2_2^+)$ is possible, there is no clear sign of the corresponding 0.92 MeV γ -ray transition to the $^{18}\text{C}(2_1^+)$ state (inset Fig. 1(b)), nor the neutron decays of comparable strength predicted to $^{18}\text{C}(0_1^+)$ and (2_1^+) – $E_{\text{rel}} = 3.34$ and 1.74 MeV, respectively.

The only other bound state(s) known in ^{18}C ($S_n = 4.18(3)$ MeV [16]) lies at 4.0 MeV with a probable $(2, 3)^+$ assignment [19,52]. The shell model suggests that decay to this level(s) may occur and would place the $3/2^-$ state at 5.42 MeV. In this case the 2.4 MeV γ -ray transition to the $^{18}\text{C}(2_1^+)$ state could be difficult to identify owing to the detection efficiency. In addition, the direct neutron decay branch to the ^{18}C ground state would be very difficult to observe owing to the low detection efficiency and poor resolution at high E_{rel} . Such a scenario is, however, complicated by the two-neutron decay to ^{17}C being also energetically possible by 0.66 MeV.

It is clear that a more detailed investigation with a higher statistics data set is desirable. While it is not possible to provide a definitive conclusion, it is probable that the $E_{\text{rel}} = 0.84$ MeV peak arises from the neutron decay of the $3/2^-$ level to a bound excited state of ^{18}C . As such, the $3/2^-$ state may be expected to lie between 3 MeV and 5.5 MeV excitation energy in ^{19}C .

Fig. 4 displays a comparison of the energies of states observed in ^{19}C (present work and Refs. [19–21,24]) with a range of different shell-model predictions. All of the calculations were, except those labeled CCEI, performed using the NuShellX@MSU code. Results are shown for the WBP, WBT [38], and YSOX [12] interactions in the p - sd model space. The results of calculations performed within the sd shell-model space utilizing the *ab initio* Coupled-Cluster Effective Interaction (CCEI) are also shown [10]. In the case of the

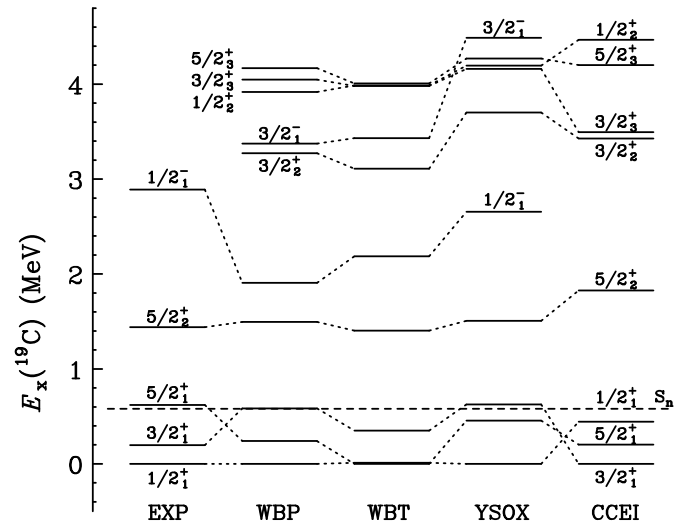


Fig. 4. Energies of states observed in ^{19}C (EXP: present work and Refs. [19–21,24]) as compared to shell-model predictions ($E_x < 5$ MeV) for states with $J^\pi \leq 5/2^+$ and $3/2^-$ using the WBP, WBT [38], YSOX [12], and CCEI [10] interactions. The latter are confined to $1s0d$ -shell states only.

YSOX interaction, the p - sd cross-shell components of the effective interaction were constructed based on V_{MU} [11], which was developed from data obtained closer to stability. The CCEI interaction includes explicitly the effects of three-body forces derived from chiral effective-field theory.

While all of the models predict the occurrence of three very low-lying positive parity states ($1/2^+$, $3/2^+$, and $5/2^+$) none is able to reproduce the ordering. Interestingly, although the CCEI shell-model calculations predict the ordering of the $3/2^+$ and $5/2^+$ levels, the $1/2^+$ state is found to lie above both of them. However, as noted by Jansen et al. [10], the very weakly bound s -wave character of the $1/2^+$ state means that the effects of the coupling to the continuum need to be properly included. Indeed, initial estimates suggest that after doing so the $1/2^+$ level is expected to be lowered, relative to the $3/2^+$ and $5/2^+$ states, by around 1 MeV. It is worthwhile noting that the spacing between the $1/2_1^+$ and $5/2_1^+$ states reflects the behavior of the corresponding neutron single-particle orbits, which are, as noted earlier, expected to be almost degenerate in the very neutron-rich carbon isotopes [19].

The newly observed $1/2^-$ state at 2.89 MeV is best accounted for by the calculations employing the YSOX interaction. This may be attributable to the cross-shell parts of the interaction incorporating V_{MU} . Such an ability to describe neutron cross-shell states in neutron-rich nuclei has also been noted in terms of the role of microscopic three-body forces, for the V_{MU} -based shell-model interaction SDPF-MU [53], which was constructed in the sd - pf model space and used to investigate the spectroscopy of $^{35,37,39}\text{Si}$ [54].

Recently, Hoffman et al. [55] have discussed the behavior of neutron s -wave states in the context of finite binding effects which become significant for shallow binding. The present study provides a measure of the relative $1/2^+ - 5/2^+$ separation in ^{19}C of $-0.62(9)$ MeV which is close to that expected on the basis of the systematics (see Fig. 4 (a) of Ref. [55]). This behavior may also be seen in the manner in which the energy of the $1/2^+$ level drops relative to that of the $5/2^+$ level in the carbon isotopes as compared to the corresponding oxygen isotones. Specifically, the $1/2^+ - 5/2^+$ separation is reduced, by an almost constant amount, for the $N = 9, 11$, and 13 isotones: 1.611(2) [49,56], 1.585(3) [51, 57], and 1.84(9) [58] MeV, respectively. It is worthwhile noting

that the lowering of the neutron $s_{1/2}$ state relative to $d_{5/2}$ state as the dripline is approached is expected for a simple potential [59], and is further enhanced by the effects of weak binding [60] as argued for by Ref. [55].

Finally it is interesting to observe that the $5/2^+$ states in ^{19}C and ^{23}O [61,62] (both $T_z = 7/2$) are each narrow resonances lying only around 50 keV above the neutron decay threshold. This is somewhat surprising as ^{23}O has a deeper neutron binding potential well $-E_x(5/2^+) - E_x(1/2^+) \approx 2.8$ MeV. Whether such behavior is a coincidence or has an underlying explanation would be interesting to investigate further.

In conclusion, single-neutron knockout from ^{20}C has been measured at 280 MeV/nucleon and three unbound levels observed in ^{19}C . Hole states $-J^\pi = 5/2^+$ and $1/2^-$ – created by removing neutrons from the $0d_{5/2}$ and $0p_{1/2}$ orbits were populated and identified by the associated longitudinal momentum distributions. Comparison with eikonal-model reaction calculations permitted spectroscopic factors to be deduced which were found to be in reasonable accord with shell-model calculations. The large spectroscopic strength observed for the population of the $5/2^+$ state indicates that the ^{20}C ground state valence neutron configuration includes, in addition to the known $1s_{1/2}^2$ component, a significant $0d_{5/2}^2$ contribution. In terms of the level scheme of ^{19}C , the YSOX interaction, developed from the monopole-based universal interaction, provided the best description, including, most notably, the energy of the newly observed $1/2^-$ cross-shell state. In this context, determining the location of the corresponding $3/2^-$ level, which would appear to lie higher in excitation energy, would be of considerable interest.

Acknowledgements

We are grateful to Dr. C. Yuan for providing us with their shell-model interaction, and to Prof. J.A. Tostevin for fruitful discussions. The work presented here was in part supported by the WCU (R32-2008-000-10155-0) and the GPF (NRF-2011-0006492) programs of NRF Korea, JSPS KAKENHI Grant Number 16H02179 and MEXT KAKENHI Grant Number 24105005 in Japan, and the French ANR grant EXPAND (ANR-14-CE33-0022-01). N.L.A., F.D., J.G., F.M.M., and N.A.O. acknowledge partial support from the French–Japanese LIA-International Associated Laboratory for Nuclear Structure Problems. A.N. and J.G. would like to acknowledge the JSPS Invitation fellowship program for long term research in Japan at the Tokyo Institute of Technology and RIKEN, respectively. S.L. gratefully acknowledges the support provided by the RIKEN International Associate Program and the hospitality of the Nishina Center Staff during his sojourn.

References

[1] I. Talmi, I. Unna, Phys. Rev. Lett. 4 (1960) 469.

[2] I. Talmi, Rev. Mod. Phys. 34 (1962) 704.
[3] D. Suzuki, et al., Phys. Rev. Lett. 103 (2009) 152503.
[4] P.A. Lunderberg, et al., Phys. Rev. Lett. 108 (2012) 142503.
[5] Z. Kohley, et al., Phys. Rev. Lett. 110 (2013) 152501.
[6] C. Caesar, et al., Phys. Rev. C 88 (2013) 034313.
[7] Y. Kondo, et al., Phys. Rev. Lett. 116 (2016) 102503.
[8] A. Volya, V. Zelevinsky, Phys. Rev. Lett. 94 (2005) 052501.
[9] G. Hagen, et al., Rep. Prog. Phys. 77 (2014) 096302.
[10] G.R. Jansen, et al., Phys. Rev. Lett. 113 (2014) 142502.
[11] T. Otsuka, et al., Phys. Rev. Lett. 104 (2010) 012501.
[12] C. Yuan, et al., Phys. Rev. C 85 (2012) 064324.
[13] D. Bazin, et al., Phys. Rev. Lett. 74 (1995) 3569.
[14] F.M. Marqués, et al., Phys. Lett. B 381 (1996) 407.
[15] T. Baumann, et al., Phys. Lett. B 439 (1998) 256.
[16] M. Wang, et al., Chin. Phys. C 36 (2012) 1603.
[17] T. Nakamura, et al., Phys. Rev. Lett. 83 (1999) 1112.
[18] V. Maddalena, et al., Phys. Rev. C 63 (2001) 046013.
[19] M. Stanoiu, et al., Phys. Rev. C 78 (2008) 034315.
[20] Z. Elekes, et al., Phys. Lett. B 614 (2005) 174.
[21] Y. Satou, et al., Phys. Lett. B 660 (2008) 320.
[22] A. Ozawa, et al., Phys. Rev. C 84 (2011) 064315.
[23] N. Kobayashi, et al., Phys. Rev. C 86 (2012) 054604.
[24] M. Thoennessen, et al., Nucl. Phys. A 912 (2013) 1.
[25] K. Whitmore, et al., Phys. Rev. C 91 (2015) 041303.
[26] Zs. Vajta, et al., Phys. Rev. C 91 (2015) 064315.
[27] Y. Kucuk, J.A. Tostevin, Phys. Rev. C 89 (2014) 034607.
[28] Y. Togano, et al., Phys. Lett. B 761 (2016) 412.
[29] Y. Yano, Nucl. Instrum. Methods Phys. Res., Sect. B 261 (2007) 1009.
[30] T. Kubo, Nucl. Instrum. Methods Phys. Res., Sect. B 204 (2003) 97.
[31] T. Kobayashi, et al., Nucl. Instrum. Methods Phys. Res., Sect. B 317 (2013) 294.
[32] T. Nakamura, Y. Kondo, Nucl. Instrum. Methods Phys. Res., Sect. B 376 (2015) 156.
[33] S. Takeuchi, et al., Nucl. Instrum. Methods Phys. Res., Sect. A 763 (2014) 596.
[34] J.A. Tostevin, J. Phys. G, Nucl. Part. Phys. 25 (1999) 735.
[35] S.D. Pain, et al., Phys. Rev. Lett. 96 (2006) 032502.
[36] A.M. Lane, R.G. Thomas, Rev. Mod. Phys. 30 (1958) 257.
[37] Y. Satou, et al., Phys. Lett. B 728 (2014) 462.
[38] E.K. Warburton, B.A. Brown, Phys. Rev. C 46 (1992) 923.
[39] L.K. Fifield, et al., Nucl. Phys. A 385 (1982) 505.
[40] P.G. Hansen, J.A. Tostevin, Annu. Rev. Nucl. Part. Sci. 53 (2003) 219.
[41] A.E.L. Dieperink, T. de Forest, Phys. Rev. C 10 (1974) 543.
[42] B.A. Brown, W.D.M. Rae, Nucl. Data Sheets 120 (2014) 115.
[43] C.A. Bertulani, A. Gade, Comput. Phys. Commun. 175 (2006) 372.
[44] A. Gade, et al., Phys. Rev. C 77 (2008) 044306.
[45] L. Ray, Phys. Rev. C 20 (1979) 1857.
[46] B.A. Brown, Phys. Rev. C 58 (1998) 220.
[47] E. Sauvan, et al., Phys. Rev. C 69 (2004) 044603.
[48] F. Carstoiu, et al., Phys. Rev. C 70 (2004) 054602.
[49] F. Ajzenberg-Selove, Nucl. Phys. A 523 (1991) 1.
[50] R. Harkewicz, et al., Phys. Rev. C 44 (1991) 2365.
[51] H. Ueno, et al., Phys. Rev. C 87 (2013) 034316.
[52] Y. Kondo, et al., Phys. Rev. C 79 (2009) 014602.
[53] Y. Utsuno, et al., Phys. Rev. C 86 (2012) 051301.
[54] S.R. Stroberg, et al., Phys. Rev. C 91 (2015) 041302.
[55] C.R. Hoffman, B.P. Kay, J.P. Schiffer, Phys. Rev. C 89 (2014) 061305.
[56] D.R. Tilley, H.R. Weller, C.M. Cheves, Nucl. Phys. A 564 (1993) 1.
[57] D.R. Tilley, et al., Nucl. Phys. A 595 (1995) 1.
[58] M. Stanoiu, et al., Phys. Rev. C 69 (2004) 034312.
[59] D.J. Millener, Nucl. Phys. A 693 (2001) 394.
[60] I. Tanihata, J. Phys. G, Nucl. Part. Phys. 22 (1996) 157.
[61] A. Schiller, et al., Phys. Rev. Lett. 99 (2007) 112501.
[62] K. Tshoo, et al., Phys. Lett. B 739 (2014) 19.